Anal. Chem. **2007,** *79,* 8098−8106

Laser Ablation Electrospray Ionization for Atmospheric Pressure, in Vivo, and Imaging Mass Spectrometry

Peter Nemes and Akos Vertes*

W. M. Keck Institute for Proteomics Technology and Applications, Department of Chemistry, George Washington University, Washington, DC 20052

Mass spectrometric analysis of biomolecules under ambient conditions promises to enable the in vivo investigation of diverse biochemical changes in organisms with high specificity. Here we report on a novel combination of infrared laser ablation with electrospray ionization (LAESI) as an ambient ion source for mass spectrometry. As a result of the interactions between the ablation plume and the spray, LAESI accomplishes electrospray-like ionization. Without any sample preparation or pretreatment, this technique was capable of detecting a variety of molecular classes and size ranges (up to 66 kDa) with a detection limit of 8 and 25 fmol for verapamil and reserpine, respectively, and quantitation capabilities with a four-decade dynamic range. We demonstrated the utility of LAESI in a broad variety of applications ranging from plant biology to clinical analysis. Proteins, lipids, and metabolites were identified, and antihistamine excretion was followed via the direct analysis of bodily fluids (urine, blood, and serum). We also performed in vivo spatial profiling (on leaf, stem, and root) of metabolites in a French marigold (*Tagetes patula*) seedling.

Mass spectrometry (MS) plays a major role in chemical, biological, and geological research. Proteomic, glycomic, lipidomic, and metabolomic studies would be impossible without modern mass spectrometry. Because of their high sensitivity and exceptional specificity, mass spectrometric methods also appear to be ideal tools for in vivo analysis in the life sciences. In many of these applications, however, the samples must be preserved in their native environment with preferably no or minimal interference from the analysis. For most of the traditional ion sources applied in the biomedical field, such as matrix-assisted laser desorption ionization (MALDI) or electrospray ionization (ESI), these limitations present serious obstacles. For example, MALDI with ultraviolet laser excitation requires the introduction of an external, often denaturing, matrix; whereas, ESI calls for liquid samples with moderate ionic conductivity. As living organisms are typically disrupted by such preparations, there is a great interest in developing direct sampling and ambient ionization sources for in vivo studies.[1]

Rapid advances in recent years have provided a growing number of ambient ion sources. For example, atmospheric pressure infrared MALDI (AP IR-MALDI), capable of producing ions from small and moderate size molecules (up to 3 000 Da), shows promise for metabolic imaging.[2] Small molecules have been analyzed by other methods, including direct analysis in real time (DART),[3,4] desorption electrospray ionization (DESI),[5] desorption atmospheric pressure chemical ionization (DAPCI),[6] and matrix-assisted laser desorption electrospray ionization (MALDESI).[7] Medium to large biomolecules have also been detected by DESI and on dehydrated samples by electrospray laser desorption ionization (ELDI).[8] Imaging capabilities were demonstrated for DESI on a rat brain tissue section with ∼400 μm lateral resolution.[9] In DESI imaging, however, depending on the analyte and surface properties, compounds might be spread to neighboring areas as a result of the washing effect.[10] Because of the need for sample pretreatment (MALDESI and to some degree ELDI), sensitivity to surface properties (DESI, DART, DAPCI, and AP IR-MALDI), and the requirement for an external matrix (MALDESI), in vivo capabilities appear to be limited for these techniques. A comparison of the analytical figures of merit, capabilities, and limitations of these emerging methods is shown in Table 1. Clearly, not all capabilities for all of the methods have been tested. From the available information it appears that all of these methods show strengths for particular applications and are prone to weaknesses in others. It is likely that eventually some subset of these techniques will prevail and complement each other as ambient ion sources.

* Corresponding author. E-mail: vertes@gwu.edu.

(1) Cooks, R. G.; Ouyang, Z.; Takats, Z.; Wiseman, J. M. *Science* **2006**, *311*, 1566−1570.
(2) Li, Y.; Shrestha, B.; Vertes, A. *Anal. Chem.* **2007**, *79*, 523−532.
(3) Cody, R. B.; Laramee, J. A.; Durst, H. D. *Anal. Chem.* **2005**, *77*, 2297−2302.
(4) Pierce, C. Y.; Barr, J. R.; Cody, R. B.; Massung, R. F.; Woolfitt, A. R.; Moura, H.; Thompson, H. A.; Fernandez, F. M. *Chem. Commun.* **2007**, 807−809.
(5) Takats, Z.; Wiseman, J. M.; Gologan, B.; Cooks, R. G. *Science* **2004**, *306*, 471−473.
(6) Takats, Z.; Cotte-Rodriguez, I.; Talaty, N.; Chen, H. W.; Cooks, R. G. *Chem. Commun.* **2005**, 1950−1952.
(7) Sampson, J. S.; Hawkridge, A. M.; Muddiman, D. C. *J. Am. Soc. Mass Spectrom.* **2006**, *17*, 1712−1716.
(8) Huang, M. Z.; Hsu, H. J.; Lee, L. Y.; Jeng, J. Y.; Shiea, L. T. *J. Proteome Res.* **2006**, *5*, 1107−1116.
(9) Ifa, D. R.; Wiseman, J. M.; Song, Q. Y.; Cooks, R. G. *Int. J. Mass Spectrom.* **2007**, *259*, 8−15.
(10) Van Berkel, G. J.; Kertesz, V. *Anal. Chem.* **2006**, *78*, 4938−4944.

10.1021/ac071181r CCC: $37.00
Published on Web 09/27/2007

Table 1. Comparison of Emerging Ambient Ionization Method Capabilities and Limitations

method	high mass limit	LOD[a]	quantitation; dynamic range	imaging; lateral resolution[b]	in vivo	limitations
DART[3]	~1 kDa	7 fmol	with internal standard	N/A[c]	N/A	limited *m/z*
DESI[5]	66 kDa	4 fmol[6]	yes; N/A	yes; 200−400 μm[10]	yes	sensitive to the surface; ill-defined sampling area; analyte washing effect
ELDI[8, 24]	66 kDa	20 fmol	N/A	N/A	N/A	sample pretreatment necessary
AP IR-MALDI[2]	~3 kDa	1 fmol/pixel	semiquantitative; 1.5 decades	40 μm with oversampling	N/A	limited *m/z*
LAESI	66 kDa	8 fmol	yes; 4 decades	300−400 μm	yes	water rich target needed

[a] Unless otherwise stated, limits of detection in this table represent the smallest total amount of analyte on the surface. For laser based methods, sometimes much better LODs are reported based on estimates of analyte amounts in the area interrogated by a laser pulse. [b] Represents a tradeoff between the sampled area and the sensitivity of the mass spectrometer. For laser based methods, in principle, it can approach the diffraction limit. [c] Not available.

Laser ablation of water-rich targets in the mid-infrared region (2.94 μm) has been utilized in medical (laser surgery)[11,12] and analytical applications both in vacuum[13,14] and at reduced[15] and atmospheric pressures (AP IR-MALDI).[2,16] In these experiments, laser energy is coupled into the target through the strong absorption band due to the OH vibrations. Ablation experiments on water, liver, and skin revealed two partially overlapping phases.[12] During the first ~1 μs, a dense plume develops as a consequence of surface evaporation and more importantly phase explosion in the target.[17] This plume contains ions, neutrals, and some particulate matter and exhibits a shock front at the plume−air interface. Its expansion is slowed by the pressure of the background gas (air); thus, it eventually comes to a halt and collapses back onto the target. The second phase is induced by the recoil pressure in the target and results in the ejection of mostly particulate matter. With dependence on the laser fluence and target properties, this phase lasts for up to ~300 μs. Very importantly, the particulates ejected in this second phase are significantly larger and thus travel to larger distances.[12]

Ultraviolet (UV) laser desorption studies in the literature on strongly absorbing targets (e.g., MALDI) in a vacuum environment indicated that the degree of ionization in the plume was between 10^{-3} and 10^{-5}.[18−20] Laser ablation in the IR is likely to produce even lower ion yields due to the lower photon energies, typically lower absorption coefficients, and the copious ejection of neutral particulates. As a consequence, the sensitivity in mass spectrometric applications suffers and the ion composition in the plume can be markedly different from the makeup of the target.

These problems can be alleviated by utilizing the neutral molecular species in the plume through postionization strategies. For example, at atmospheric pressure, applying a radioactive β emitter (e.g., a ^{63}Ni foil)[21] or chemical ionization through a corona discharge[22,23] improved the ion yields for low-mass molecules. In a recent breakthrough, the ELDI method combined UV laser ablation with ESI.[24] Significantly, ELDI did not exhibit significant discrimination against high mass analytes up to ~20 kDa.[8]

In this contribution, we report on the combination of mid-infrared laser ablation with electrospray ionization (LAESI) as a novel ion source for mass spectrometry under ambient conditions. We explore the use of LAESI in the direct analysis of assorted samples from diverse surfaces for small organic molecules and biomolecules as large as 66 kDa. LAESI is applied for the ambient analysis of complex biological fluids and tissue samples with water content. We demonstrate the in vivo spatial profiling of a French marigold (*Tagetes patula*) seedling by LAESI mass spectrometry. Metabolites specific to the leaf, the stem, and the root of the plant are distinguished. Insight into the LAESI mechanism is gained by fast imaging of the interacting laser ablation and electrospray plumes.

METHODS

Laser Ablation Electrospray Ionization. The electrospray system was identical to the one described in an earlier study.[25] Briefly, 50% methanol solution containing 0.1% (v/v) acetic was fed through a tapered tip metal emitter (100 μm i.d. and 320 μm o.d., New Objective, Woburn, MA) using a low-noise syringe pump (Physio 22, Harvard Apparatus, Holliston, MA). Stable high voltage was directly applied to the emitter by a regulated power supply (PS350, Stanford Research Systems, Inc., Sunnyvale, CA). A flat polished stainless steel plate counter electrode (38.1 mm × 38.1 mm × 0.6 mm) with a 6.0 mm diameter opening in the center was placed perpendicular to the axis of the emitter at a distance of 10 mm from the tip. This counter electrode was used to monitor the spray current with a digital oscilloscope (WaveSurfer 452, LeCroy, Chestnut Ridge, NY). The temporal behavior of the spray current was analyzed to determine the established spraying mode. The flow rate and the spray voltage were adjusted to establish

(11) Vogel, A.; Venugopalan, V. *Chem. Rev.* **2003**, *103*, 577−644.
(12) Apitz, I.; Vogel, A. *Appl. Phys. A: Mate. Sci. Process.* **2005**, *81*, 329−338.
(13) Berkenkamp, S.; Karas, M.; Hillenkamp, F. *Proc. Natl. Acad. Sci. U.S.A.* **1996**, *93*, 7003−7007.
(14) Leisner, A.; Rohlfing, A.; Berkenkamp, S.; Hillenkamp, F.; Dreisewerd, K. *J. Am. Soc. Mass Spectrom.* **2004**, *15*, 934−941.
(15) Dreisewerd, K.; Draude, F.; Kruppe, S.; Rohlfing, A.; Berkenkamp, S.; Pohlentz, G. *Anal. Chem.* **2007**, *79*, 4514−4520.
(16) Laiko, V. V.; Taranenko, N. I.; Berkout, V. D.; Yakshin, M. A.; Prasad, C. R.; Lee, H. S.; Doroshenko, V. M. *J. Am. Soc. Mass Spectrom.* **2002**, *13*, 354−361.
(17) Chen, Z. Y.; Bogaerts, A.; Vertes, A. *Appl. Phys. Lett.* **2006**, *89*.
(18) Ens, W.; Mao, Y.; Mayer, F.; Standing, K. G. *Rapid Commun. Mass Spectrom.* **1991**, *5*, 117−123.
(19) Mowry, C. D.; Johnston, M. V. *Rapid Commun. Mass Spectrom.* **1993**, *7*, 569−575.
(20) Puretzky, A. A.; Geohegan, D. B. *Chem. Phys. Lett.* **1998**, *286*, 425−432.
(21) Kolaitis, L.; Lubman, D. M. *Anal. Chem.* **1986**, *58*, 2137−2142.
(22) Coon, J. J.; Harrison, W. W. *Anal. Chem.* **2002**, *74*, 5600−5605.
(23) Coon, J. J.; McHale, K. J.; Harrison, W. W. *Rapid Commun. Mass Spectrom.* **2002**, *16*, 681−685.
(24) Shiea, J.; Huang, M. Z.; Hsu, H. J.; Lee, C. Y.; Yuan, C. H.; Beech, I.; Sunner, J. *Rapid Commun. Mass Spectrom.* **2005**, *19*, 3701−3704.
(25) Nemes, P.; Marginean, I.; Vertes, A. *Anal. Chem.* **2007**, *79*, 3105−3116.

the cone−jet regime.[25,26] The electrohydrodynamic behavior of the Taylor cone and the plume of ablated particulates were followed by a fast digital camera (QICAM, QImaging, Burnaby, BC, Canada) equipped with a long-distance microscope (KC, Infinity Photo-Optical Co., Boulder, CO). The cone and the generated droplets were back-illuminated with a ~10 ns flash source[25] based on fluorescence from a laser dye solution (Coumarin 540A, Exciton, Dayton, OH) excited by a nitrogen laser (VSL-337, Newport Corp., Irvine, CA).

The samples were mounted on microscope slides, positioned 10−30 mm below the spray axis and 3−5 mm ahead of the emitter tip, and ablated at a 90° incidence angle using an Er:YAG laser (Bioscope, Bioptic Lasersysteme AG, Berlin, Germany) at a wavelength of 2940 nm. The Q-switched laser source with a pulse length of <100 ns was operated at 5 Hz repetition rate with an average output energy of 3.5 mJ/shot and a 4% pulse energy stability. Focusing was achieved by a single planoconvex CaF_2 lens ($f = 150$ mm). Burn marks on a thermal paper (multigrade IV, Ilford Imaging Ltd., UK) indicated that the laser spot was circular with a diameter of 350−400 μm, and its size did not change appreciably by moving the target within ~20 mm around the focal distance. This corresponded to ~2.8−3.6 J/cm^2 laser fluence that could result in >60 MPa recoil stress buildup in the target.[27]

The material expelled by the recoil pressure due to laser ablation was intercepted by the electrospray plume operating in the cone−jet mode, and the generated ions were mass analyzed with an orthogonal acceleration time-of-flight (oa-TOF) mass spectrometer (JMST100LC AccuTOF, JEOL Ltd., Peabody, MA). The data acquisition rate was set to 1 s/spectrum. By adjustment of the sampling cone to skimmer potential difference, the sampled ions could undergo collision induced dissociation (CID) in the ion source of the instrument, at an intermediate pressure of ~150 Pa. The structurally meaningful fragments produced in such in-source CID experiments were useful in identifying some of the analytes, without the need of a regular CID cell. The AccuTOF mass spectrometer allowed us to increase the accuracy of mass measurements by using internal mass calibration. In these so-called "drift compensation measurements", the mass of the internal standard was drifted to its calculated monoisotopic mass, providing better mass accuracy for unknown ions with similar masses. The sampling cone of the mass spectrometer was in line with the spray axis. The ion optics settings were optimized for the analyte of interest and were left unchanged during consecutive experiments. The LAESI system was shielded by a Faraday cage and a plastic enclosure to minimize the interference of electromagnetic fields and air currents, respectively. The enclosure also provided protection from the health hazards of the fine particulates generated in the laser ablation process.

To expose fresh areas during data acquisition, some of the samples were raster scanned by moving them in the $X-Y$ plane in front of the laser beam using an $X-Y-Z$ translation stage. Unless otherwise mentioned, the presented mass spectra were averaged over 5 s (25 laser shots). Frequently, single laser shots also gave sufficient signal-to-noise ratio (S/N > 3) in the mass spectra. The LAESI experiments were followed by microscope inspection and imaging of the ablation spots on the targets.

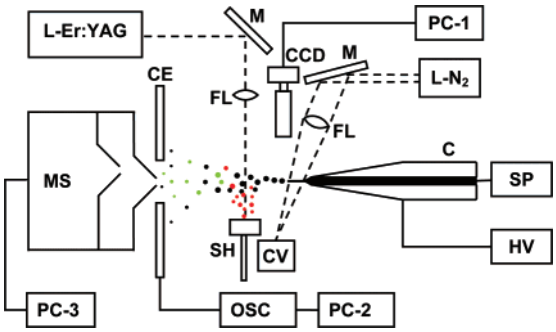

Figure 1. Schematics of laser ablation electrospray ionization (LAESI) and fast imaging system (C, capillary; SP, syringe pump; HV, high-voltage power supply; L-N_2, nitrogen laser; M, mirrors; FL, focusing lenses; CV, cuvette; CCD, CCD camera with short-distance microscope; CE, counter electrode; OSC, digital oscilloscope; SH, sample holder; L-Er:YAG, Er:YAG laser; MS, mass spectrometer; PC-1 to PC-3, personal computers). The cone−jet regime is maintained through monitoring the spray current on CE and adjusting the spray parameters. Black dots represent the droplets formed by the electrospray. Their interaction with the particulates and neutrals (red dots) emerging from the laser ablation produces some fused particles (green dots) that are thought to be the basis of the LAESI signal.

French Marigold Plant. French marigold (*Tagetes patula*) seeds were obtained from Fisher Scientific. Seedlings were grown in artificial medium in a germination chamber (model S79054, Fisher Scientific). Two seedlings were removed at 2 and 4 weeks of age and were subjected to LAESI analysis without any chemical pretreatment. The roots of the plants were kept moist to avoid wilting during the studies. Following the experiment, the plants were transplanted into soil and their growth was monitored for up to an additional 4 weeks to confirm viability.

RESULTS

Postionization in Atmospheric Pressure Infrared Laser Ablation. Encouraged by the success of ELDI on pretreated and/or dehydrated samples, we sought to develop a new ionization technique for the analysis of untreated water-rich biological samples under ambient conditions. Similarly to AP IR-MALDI,[2] in LAESI, mid-IR laser ablation was used to produce a plume directly from the target. To postionize the neutrals and the particulate matter, this plume was intercepted under at a right angle by an electrospray operating in the cone−jet regime.[25] Figure 1 shows the schematics of the experimental arrangement. We chose the cone−jet spraying regime because of its exceptional ion yield and elevated duty cycle compared to other (e.g., burst or pulsating) modes of ESI operation.[25,26,28,29] The sampling orifice of the mass spectrometer was in line with the spray axis. With the spray operating, laser ablation of targets absorbing in the mid-IR resulted in abundant ion signal over a wide range of m/z values. With no solution pumped through the electrified or floating emitter, no analyte ions were detected upon laser ablation. Thus LAESI is genuinely different from AP IR-MALDI in the origin of the ion signal. Conversely, with the spray present but without laser

(26) Valaskovic, G. A.; Murphy, I. J. P.; Lee, M. S. *J. Am. Soc. Mass Spectrom.* **2004**, *15*, 1201−1215.
(27) Venugopalan, V.; Nishioka, N. S.; Mikic, B. B. *Biophys. J.* **1996**, *70*, 2981−2993.
(28) Marginean, I.; Parvin, L.; Heffernan, L.; Vertes, A. *Anal. Chem.* **2004**, *76*, 4202−4207.
(29) Marginean, I.; Nemes, P.; Vertes, A. *Phys. Rev. Lett.* **2006**, *97*, 064502.

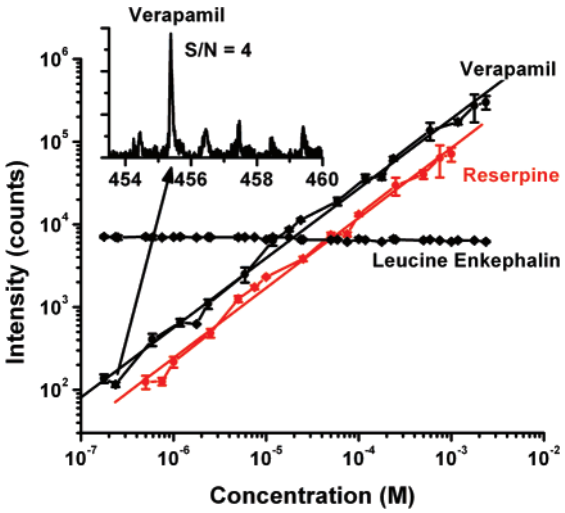

Figure 2. Figures of merit for LAESI-MS. Solutions containing verapamil and reserpine at various concentrations (10^{-9} to 2.36×10^{-3} M) were prepared with 50% methanol (0.1% acetic acid). A leucine enkephalin solution of constant concentration (0.5 μM) was electrosprayed to monitor the stability of the electrospray (◆). Aliquots of 5 μL were presented for LAESI-MS analysis. Mass spectra were averaged over 15 s (~75 laser pulses), and each experiment was repeated three times. The relative configuration of the LAESI source was kept unchanged during the analysis. The measured abundance of verapamil (black filled circles) and reserpine (red filled circles) were plotted against their concentrations on a log−log scale. The linear regression equations and the correlation coefficients for verapamil and reserpine were log(intensity/counts) = 7.8 + 0.84 log($c_{verapamil}$/M); $R_{verapamil}$ = 0.996, and log(intensity/counts) = 7.5 + 0.85 log($c_{reserpine}$/M); $R_{reserpine}$ = 0.995, respectively. The ablated volume was estimated from the weight loss of the sample as 0.5 μL. Limits of detection (at S/N = 4) for verapamil (2.36×10^{-7} M) (the corresponding spectrum is shown in the inset) and reserpine (7.5×10^{-7} M) were determined at 8 and 25 fmol, respectively.

ablation no sample-related analyte ion signal was observed (solvent-related ions from the electrospray were, however, present). Thus, a DESI-like scenario, or one involving chemical ionization through corona discharge at the emitter, did not play a role in the ionization process. As we demonstrate after the discussion of concrete applications, LAESI also bears major differences from ELDI in both the range of its utility and probably in the details of ion production.

Analytical Figures of Merit. The figures of merit for LAESI were encouraging. A series of analyte solutions containing both verapamil and reserpine at concentrations ranging from 1 nM to 10 mM were prepared with 50% methanol acidified with 0.1% acetic acid. Aliquots of 5 μL of these solutions were analyzed by LAESI mass spectrometry over 15 s (75 laser pulses). A 50% acidified methanol solution (0.1% acetic acid) was electrosprayed in the cone−jet spraying mode. Leucine enkephalin was also added to this solution at 0.5 μM concentration to monitor the stability of the spray by following the protonated leucine enkephalin abundance. As it is shown in Figure 2, linear correlation was observed between the measured abundance for $[verapamil + H]^+$ and $[reserpine + H]^+$ and their concentrations. The linear regression in Figure 2 yielded a correlation coefficient of at least 0.995 for both analytes. The signal was integrated for 1 s (i.e., 5 laser shots), and limits of detection of 8 and 25 fmol were determined for verapamil and reserpine, respectively. Further optimization of the LAESI source geometry can improve these numbers. Alternatively, nanoelectrospray ionization can be used, offering a better ionization yield.

For the studied compounds, LAESI showed exceptional quantitation possibilities and 4 orders of magnitude dynamic range (see Figure 2). An advantage of the method is that an internal standard is not necessary for quantitation. This is in contrast to other atmospheric pressure methodologies like the semiquantitative AP IR-MALDI, or DART, and DESI that require internal standards. Furthermore, no suppression of the studied analyte ions by each other or by the leucine encephalin introduced into the spray was observed.

The depth of the ablated crater in solids and the amount of the removed material in liquids are dependent on the laser fluence and on the optical, surface, thermal, and mechanical properties of the target. The irregular surface of tissues and their heterogeneous structure presented additional complications for determining the depth of ablation craters. On the basis of weight loss measurements, we found that 75 laser shots removed ~0.5 μL of liquid sample but this data could have been skewed due to the redeposition of some of the ablated material on the sample.

We successfully tested the use of LAESI on a variety of samples, including pharmaceuticals, small dye molecules, peptides, explosives, synthetic polymers, animal and plant tissues, etc., in both positive and negative ion modes. Here, we only present some of the examples most relevant in life sciences.

Antihistamine Excretion. Fexofenadine (molecular formula $C_{32}H_{39}NO_4$) is the active ingredient of various medications (e.g., Allegra and Telfast) for the treatment of histamine-related allergic reactions. This second-generation antihistamine does not readily enter the brain from the blood, and it therefore causes less drowsiness than other remedies. To understand the pharmacokinetics of the active ingredient, absorption, distribution, metabolism, and excretion (ADME) studies are needed. For example, radiotracer investigations show that fexofenadine is very poorly metabolized (only ~5% of the total oral dose), and the preferential route of excretion is through feces and urine (80% and 11%, respectively).[30] This and other traditional methods (e.g., liquid chromatography with MS), however, are time-consuming and require a great deal of sample preparation. As in the clinical stage of drug development, it is common to encounter the need for the analysis of 1000−10 000 samples,[31] so high throughput analysis is important. We tested whether LAESI was capable of rapidly detecting fexofenadine directly from urine without chemical pretreatment or separation.

A Telfast caplet with 120 mg of fexofenadine (FEX) was orally administered to a healthy volunteer. Urine samples were collected before and several times after ingestion. For all cases, a 5 μL aliquot of the untreated sample was uniformly spread on a microscope slide and directly analyzed by LAESI-MS. A comparison made between the LAESI mass spectra showed that new spectral features appeared after drug administration. Figure 3 shows the mass spectrum acquired 2 h after ingestion. The peaks highlighted by red ovals correspond to the protonated form and a fragment (due to water loss) of fexofenadine. Accurate mass measurements indicated the presence of an ion with m/z 502.299

(30) Molimard, M.; Diquet, B.; Benedetti, M. S. *Fundam. Clin. Pharmacol.* **2004**, *18*, 399−411.
(31) Lee, M. S.; Kerns, E. H. *Mass Spectrom. Rev.* **1999**, *18*, 187−279.

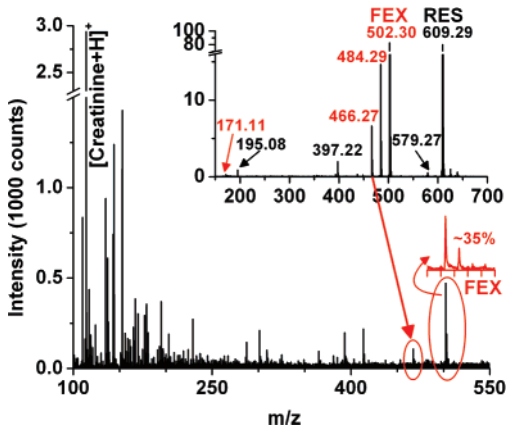

Figure 3. Excretion of the antihistamine fexofenadine (FEX) studied by LAESI mass spectrometry. A 5 μL aliquot of the urine sample collected 2 h after administering a Telfast caplet with 120 mg of fexofenadine active ingredient was directly analyzed using LAESI-MS. Compared to the reference sample taken before administering the drug, the spectra urine the presence of some new species (red ovals). Accurate mass measurements on dissolved scrapings from a caplet core (see black inset) after drift compensation for reserpine (RES) showed *m/z* 502.30 that corresponded to the elemental composition of protonated fexofenadine, $[C_{32}H_{39}NO_4 + H]^+$, with a 7.5 ppm mass accuracy. Analysis of the caplet core by LAESI-MS (black inset) showed fragments of fexofenadine (*m/z* 484.29, 466.27, and 171.11) and reserpine (*m/z* 579.27, 397.22, and 195.08). A comparison of the spectra revealed that two of the new species observed in the urine sample were the molecular ion and a fragment of fexofenadine, *m/z* 502.30 and 466.27, respectively.

that corresponded to the elemental composition $[C_{32}H_{39}NO_4 + H]^+$ with a 7.5 ppm mass accuracy. The measured ~35% intensity at M + 1 (see red inset) is consistent with the isotope abundances of this elemental composition. The mass spectra showed the presence of numerous other metabolites not related to the drug. For example, protonated ions of creatinine, the breakdown product of phosphocreatine, were very abundant. In future studies, the other numerous metabolites present can be identified through, e.g., tandem MS for broader metabolomics applications.

For reference, the caplet itself was also analyzed by LAESI (see black inset in Figure 3). A small portion of the caplet core was dissolved in 50% methanol containing 0.1% acetic acid, and reserpine (RES) was added for accurate mass measurements. The inset in Figure 3 shows that both the fexofenadine and the reserpine underwent in-source collision activated dissociation. In the inset of Figure 3, the resulting peaks are labeled in black for reserpine (RES, *m/z* 609.29) and its fragments (*m/z* 579.27, 397.22, and 195.08),[25] and in red for fexofenadine (FEX, *m/z* 502.30) and its fragments (*m/z* 484.29, 466.27, and 171.11). Two of the fexofenadine fragments (*m/z* 484.29 and 466.27) are produced from the molecular ion through consecutive water loss. A comparison of the spectra revealed that two of the new species observed in the urine sample were the molecular ion and a fragment of fexofenadine, *m/z* 502.30 and 466.27, respectively.

The quantitation capabilities of LAESI allow one to follow the excretion of fexofenadine. As no sample preparation is needed, the analysis time is limited by sample presentation (spotting on the target plate) and spectrum integration time that for individual samples take ~5 and ~1 s, respectively. For high throughput applications, the sample presentation time can be significantly reduced by sample holder arrays, e.g., 384-well plates, and robotic plate manipulation.

Whole Blood and Serum Samples. Because of the complexity of the sample, the chemical analysis of whole blood is a challenging task generally aided by separation techniques. Exceptions are the DESI and ELDI methods that have been shown to detect various molecules from moderately treated whole blood samples. In this example, we demonstrate that LAESI can detect metabolites and proteins directly from untreated whole blood samples.

Approximately 5 μL of whole blood was spread on a microscope slide and was directly analyzed by LAESI. In the mass spectra (see Figure 4a) several singly and multiply charged species were detected in the low *m/z* (<1000 Da) region. With the use of accurate mass measurements and with the aid of a human metabolome database (available at http://www.hmdb.ca/), phosphocholine (PC, see the 20× enlarged segment of the spectrum) and glycerophosphocholines (GPC) were identified. The most abundant ion corresponded to the heme group of human hemoglobin. In the mid- to high-*m/z* (>1000 Da) region, a series of multiply charged ions were observed. Their deconvolution identified them as the α- and β-chains of human hemoglobin with neutral masses of 15 127 and 15 868 Da, respectively (see the inset in Figure 4a). An unidentified protein with a neutral mass of 10 335 Da was also detected.

Lyophilized human serum, deficient in immunoglobulins, was reconstituted in deionized water and was subjected to LAESI-MS. The averaged spectrum is shown in Figure 4b. Several metabolites were detected and identified in the lower *m/z* region, including carnitine, phosphocholine (PC), tetradecenoylcarnitine (C14-carnitine), and glycerophosphocholines (GPC). On the basis of molecular mass measurements alone, the structural isomers of GPCs cannot be distinguished. With the use of tandem mass spectrometry and accurate mass measurements, however, many of these isomers and the additional species present in the spectrum can be identified. Similarly to the previous example, multiply charged ion distributions were also observed. By the deconvolution of the ions observed in the higher *m/z* region (see inset), we identified human serum albumin (HSA) with a neutral mass of 66 556 Da. These examples indicate that LAESI achieves ESI-like ionization without sample preparation and extends the mass range of the AP IR-MALDI technique. This latter aspect of LAESI is especially valuable. In AP IR-MALDI there is a strong discrimination against high mass (*m* > 3000 Da) ions.[2] Although the origin of this effect is not clear, potential explanations include rapid recombination, clustering, or decomposition of the larger ions in the AP interface. It is also possible that the transport of these ions in the intermediate pressure region of the interface is less efficient. LAESI, perhaps through the generation of multiply charged ions, effectively removes this limitation and extends the mass range to 66 kDa.

In Vivo Profiling of a Petite French Marigold. Postionization of the laser ablation plume provides LAESI with superior ionization efficiency over AP MALDI approaches. For example, we observed a ~10^2–10^4-fold enhancement in ion abundances compared to those reported for AP IR-MALDI.[2] Higher sensitivity is most beneficial for in vivo studies that usually aim at the detection of low-concentration species with minimal or no damage to the

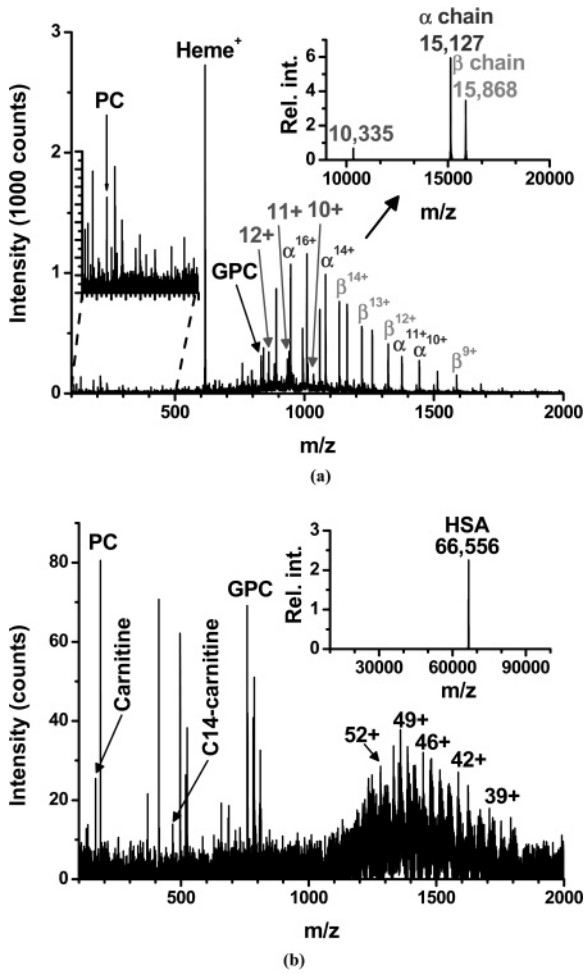

Figure 4. LAESI-MS analysis of whole blood and serum. (a) LAESI-MS spectrum of whole blood without any pretreatment showed several singly and multiply charged peaks in the low *m*/*z* (<2000 Da) region. The numbers in the spectrum, *n*+, indicate the charge states. With the use of accurate mass measurements and a human metabolome database search, phosphocholine (PC) (see the 20× enlarged segment of the spectrum) and glycerophosphocholines (GPC) were identified. The mass spectrum was dominated by the heme group of human hemoglobin ($Heme^+$). Deconvolution of the spectrum of multiply charged ions (inset) in the higher *m*/*z* region identified the α- and β-chains of human hemoglobin with neutral masses of 15 127 Da and 15 868 Da, respectively. An unidentified protein with a neutral mass of 10 335 Da was also detected. (b) Human serum deficient in immunoglobulines in LAESI-MS experiments revealed several metabolites in the lower *m*/*z* region. Carnitine, phosphocholine (PC), tetradecenoylcarnitine (C14-carnitine), and glycerophosphocholines (GPC) were identified. With accurate mass measurements and tandem mass spectrometry, these GPCs can be distinguished. Deconvolution of the multiply charged ions observed in the higher *m*/*z* region (see inset) identified human serum albumin (HSA) with a neutral mass of 66 556 Da.

organism. As an example, we utilized LAESI for the in vivo profiling of metabolites in petite French marigold seedlings. The home-grown plants were placed on a microscope slide and single-laser shot analysis was performed on the leaf, stem, and root of the plant to minimize the tissue damage.

The acquired mass spectra (see Figure 5a) revealed various metabolites at high abundances. We identified some of these compounds in a two-step process. Because of the similarity of some metabolites for a diversity of plants, we first performed a

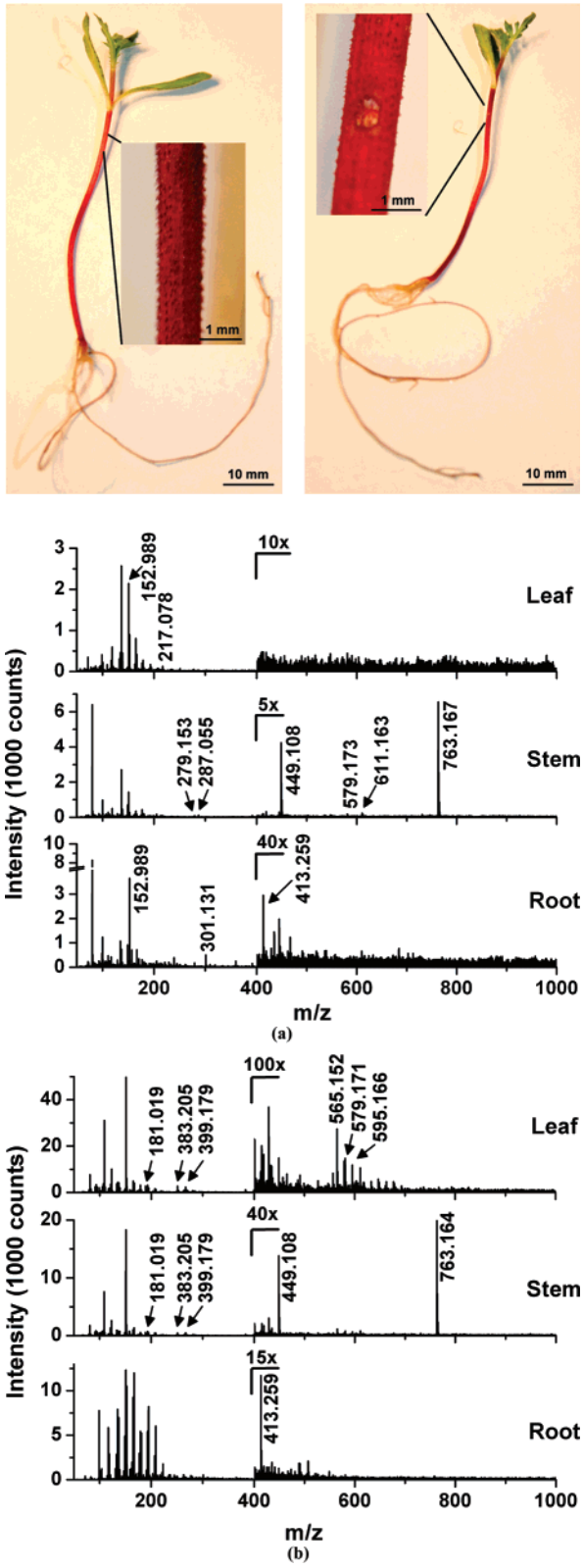

Figure 5. In-vivo identification of metabolites in French marigold (*Tagetes patula*) seedling organs by LAESI-MS. (a) Single shot laser ablation of the leaf, the stem, and the root of the plant produced mass spectra that included a variety of metabolites, some of them organ specific, detected at high abundances. Images of the analyzed area on the stem before and after the experiment showed superficial damage on a 350 μm diameter spot (see insets). (b) The signal for lower abundance species was enhanced by averaging 5−10 laser shots.

Table 2. Metabolites in French Marigold Seedling Organs Tentatively Assigned by in Vivo LAESI-MS Experiments[a]

no.	metabolite	formula	monoisotopic mass	measured mass	$\Delta m/z$ (10^{-3})	organ	metabolic pathways
1	glucose	$C_6H_{12}O_6$	181.071 (H)	181.019 (H)	52	leaf, stem	gluconeogenesis, glycolysis
2	2-*C*-methyl-erythritol-4-phosphate	$C_5H_{13}O_7P$	217.048 (H)	217.078 (H)	30	leaf	methylerythritol phosphate pathway
3	kaempferol xylosyl rhamnoside	$C_{26}H_{28}O_{14}$	565.155 (H)	565.152 (H)	3	leaf	flavonol biosynthesis
4	kaempferol-3-rhamnoside-7-rhamnoside	$C_{27}H_{30}O_{14}$	579.171 (H)	579.173 (H)	2	leaf	flavonol biosynthesis
5	kaempferol 3-*O*-rhamnoside-7-*O*-glucoside	$C_{27}H_{30}O_{15}$	595.166 (H)	595.171 (H)	5	leaf	flavonol biosynthesis
6	linolenic acid	$C_{18}H_{30}O_2$	279.232 (H)	279.153 (H)	79	stem	fatty acid oxidation
			301.214 (Na)	301.131 (Na)	83		
7	cyanidin	$C_{15}H_{11}O_6$	287.056 (+)	287.055 (+)	1	stem	anthocyanin biosynthesis, flavonol
8	luteolin, kaempferol	$C_{15}H_{10}O_6$	287.056 (H)	287.055 (H)	1		biosynthesis
	cyanidin-3-glucoside,	$C_{21}H_{21}O_{11}$	449.108 (+)	449.109 (+)	1	stem	anthocyanin biosynthesis, flavonol
	kaempferol-3-glucoside	$C_{21}H_{20}O_{11}$	449.108 (H)	449.109 (H)	1		biosynthesis
9	cyanidin-3,5-diglucoside,	$C_{27}H_{31}O_{16}$	611.161 (+)	611.163 (+)	2	stem	anthocyanin biosynthesis,
	kaempferol 3,7-*O*-diglucoside	$C_{27}H_{30}O_{16}$	611.161 (H)	611.163 (H)	2		flavonol biosynthesis
10	kaempferol 3-*O*-(2″, 3″-di-*p*-coumaroyl)-glucoside	$C_{39}H_{32}O_{15}$	763.164 (Na)	763.167 (Na)	3	stem	
11	methylsalicylate	$C_8H_8O_3$	153.055 (H)	152.989 (H)	66	root	benzenoid ester biosynthesis,
	xanthine	$C_5H_4N_4O_2$	153.041 (H)	152.989 (H)	52		ureide degradation and synthesis
12	hydroxyflavone	$C_{15}H_{10}O_3$	239.071 (H)	239.153 (H)	82	root	
	methyl-isopentenyl-adenine	$C_{12}H_{16}N_4$	239.127 (Na)	239.153 (Na)	26		
13	bestatin	$C_{16}H_{24}N_2O_4$	309.181 (H)	309.194 (H)	13	root	wound signaling
14	phytosterols	$C_{29}H_{48}O$	413.378 (H)	413.259 (H)	119	root	sterol biosynthesis

[a] The assignments are based on a combination of accurate mass measurements, metabolomic database search, isotopic distributions and, in some cases, tandem MS analysis. The symbols in parentheses, (H) and (Na), indicate protonated and sodiated species, respectively, whereas (+) stands for preformed ions.

search for the measured masses in the metabolomic database for *Arabidopsis thaliana* (available at http://www.arabidopsis.org/). In some cases isotopic distributions of ionic species with similar masses were determined to help with the assignment. The list of compounds was further extended by performing LAESI experiments, in which the mass spectra were averaged over ~5−10 consecutive laser shots in an area within 1−2 mm (see Figure 5b). Several additional compounds were detected, most likely due to the better signal-to-noise ratio provided by signal averaging.

By comparing the mass spectra obtained for the leaf, stem, and root, we found that certain metabolites were specific to the organs of the plant. The assigned compounds with the location of their occurrence and some of the related metabolic pathways are listed in Table 2. Consistent with the noncovalent hexose clusters in Figure 5b (m/z 383.205 and 399.179 correspond to the sodiated and potassiated dimers, respectively), both the leaf and the stem had a high glucose and secondary metabolite, e.g., flavonoid, content. However, different types of flavonoids were found in the leaf and the stem. The root primarily contained low-mass (m/z < 250) as yet unidentified components. Some of these components with lower abundance were also present in the other two organs of the plant.

Compounds **8** and **10** were detected at surprisingly high abundances. For the latter, however, the database search gave no results. In-source CID experiments proved that **10** had relatively high stability; therefore, the possibility of a noncovalent cluster was excluded. Accurate mass measurements gave m/z 763.167 with ~40% M + 1 isotopic distribution, which corresponded to a $C_{39}H_{32}O_{15}Na^+$ elemental composition within 4 ppm mass accuracy. Although multiple structural isomers could correspond to the same chemical formula, based on previous reports in the literature on a flavonoid of identical mass,[32] we assigned the compound as the sodiated form of kaempferol 3-*O*-(2″,3″-di-*p*-coumaroyl)-glucoside. Tandem MS results on extracts from the stem indicated the presence of several structural features consistent with this assignment. The presence of other kaempferol derivatives in the plant can also be viewed as corroborative evidence.

After the analysis, microscope examination of the stem and the leaf revealed circular ablation marks of ~350 μm in diameter (see the insets in Figure 5). This localized superficial damage had no influence on the life cycle of the seedling. We must emphasize however that due to the ablation by the IR-laser, LAESI is a destructive method; thus, the size of the sampled area (currently 350−400 μm) needs to be considered as a limiting factor for in vivo experiments. Improvements can be achieved by reducing the size of the ablated areas or applying lower laser irradiances. Selecting a lens with shorter focal length, reducing the divergence of the laser beam by a beam expander, and/or using aspherical optics can produce significantly tighter focusing (and much less damage).

LAESI Mechanism. In the LAESI experiments, surprisingly large target-to-spray distances (10−30 mm) provided the strongest signal. This is a profound departure from our findings in AP IR-MALDI, where the optimum ion signal has been obtained at 2 mm from the ablated surface.[2] A plausible explanation for this

(32) Imperato, F. *Am. Fern J.* **2003**, *93*, 157−160.

difference is that AP IR-MALDI samples the ions produced in the early phase of the plume development. This plume, however, collapses in a few microseconds and gives way to the recoil pressure induced particulate ejection. The ejected particles of this second phase travel to longer distances and have the opportunity to be engulfed by the charged droplets of the electrospray.

Indeed, following the laser pulse, often material ejection was visually observed in the form of small particulates. The optimum distance of the ablation spot to the spray axis was established as ~25 mm, but appreciable ion abundances were still measured at 30 mm and beyond. As the area of the laser spot did not change noticeably within ~20 mm of the focal distance, the variations in LAESI signal were not related to differences in laser irradiance. We also noticed that short target-to-spray distances (e.g., ~5 mm) led to the destabilization of the electrospray, resulting in a significant deterioration of the LAESI ion counts.

To confirm the interaction of the laser ablated particulates with the electrospray droplets in LAESI, flash shadowgraphy based fast imaging[25] of the anticipated interaction region was carried out with ~10 ns exposure time. Upon infrared laser ablation of the methanol solution target positioned 10 mm below and ~1 mm ahead of the emitter tip, a fine cloud consisting of clusters, nanoparticles, and particulates with a size distribution that extends up to 3 μm was produced and it was traveling vertically (from the bottom to the top in Figure 6). With our visualization method, the submicron particles were not detected. Although the low end of this size distribution is probably more significant in the analyte ion production, we observed the larger particulates to follow the evolution of the plume.

The mixture of clusters, nanoparticles, and particulates was intercepted by the electrospray plume that evolved horizontally (from left to right) at the sampling height. In the pulsating mode (see the top panel of Figure 6), the ES plume is clearly visible as it expands from the end of the filament in a conical pattern. The laser ablated particles that could be visualized are somewhat larger and enter from the bottom.

The image in the bottom panel shows the ES source operating in the cone–jet regime and producing much smaller droplets that are not resolved in the image. Here the larger laser ablated particles are clearly visible and are shown to travel through the region of the ES plume. Comparing the LAESI signal for the pulsating and cone–jet ES regimes indicated that ion production was more efficient in the latter. These images suggest that the mechanism of ion formation in LAESI involves the fusion of laser ablated nanoparticles and larger particulates with the charged ES droplets. The fused droplets are thus seeded with the analytes from the target, retain their charge, and continue their trajectory toward the mass spectrometer. Many of the ions produced from these droplets are derived from the analytes in the ablation target and exhibit the characteristics of ES ionization, e.g., multiply charged ions for peptides and proteins (see Figure 4).

These observations in combination with fast imaging results on IR-laser ablation can provide some insight into the mechanism of LAESI. At similar laser fluences, water and soft tissues first undergo nonequilibrium vaporization in the form of surface evaporation and to a much larger degree phase explosion.[17] After ~1 μs, the expansion stops at a few millimeters from the surface and the plume collapses. Because of the recoil stress in the condensed phase, secondary material ejection follows in the form of particulates[12] that can last up to several hundred microseconds. These particulates travel to larger distances than the initial plume. They are slowed and eventually stopped at tens of millimeters from the target by the drag force exerted on them by the resting background gas. The difference between the stopping distance of the primary plume and the recoil induced particle ejection can explain the difference between the optimum sampling distance for AP IR-MALDI (~2 mm)[2] and LAESI (~25 mm).

According to the fused-droplet hypothesis introduced for ELDI, a similar process is responsible for ion production in that method.[33] In ELDI, however, a UV laser is used to perform nonresonant

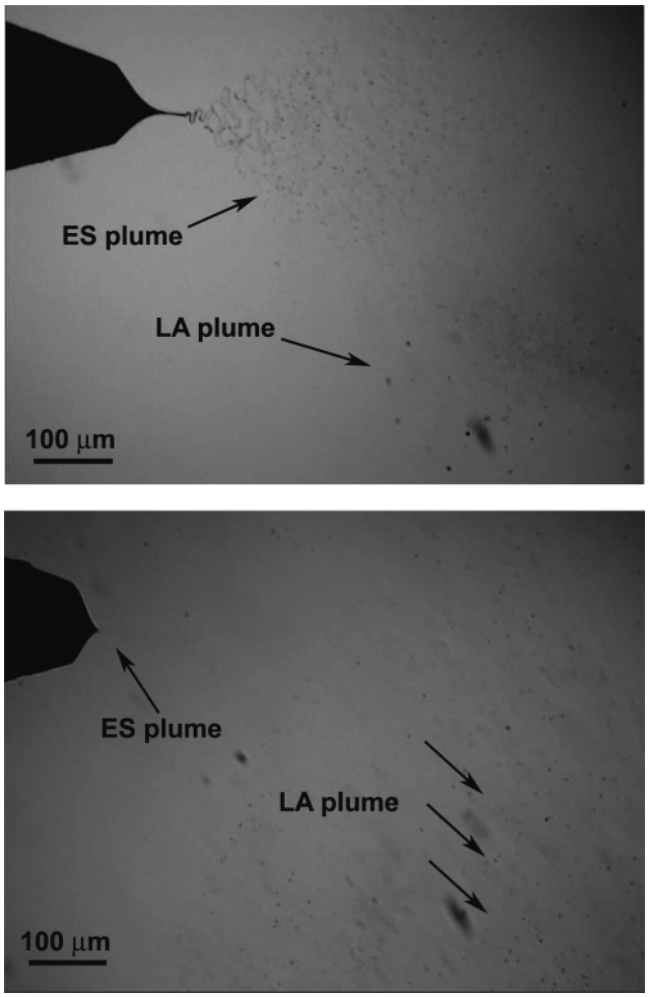

Figure 6. Flash shadowgraphy with ~10 ns exposure time reveals the interaction between the electrospray (ES) plume and the laser ablation plume (LA) in a LAESI experiment. Pulsating spraying regime (top panel) offered lower duty cycle and larger ES droplets, whereas in the cone–jet regime (bottom panel) the droplets were continuously generated and were too small to appear in the image. As the electrosprayed droplets traveled downstream from the emitter (from left to right), their trajectories were intercepted by the fine cloud of particulates (black spots in the images corresponding to 1–3 μm particles) traveling upward from the IR-ablation plume. At the intersection of the two plumes, some of the ablated particulates are thought to fuse with the ES droplets. The resulting charged droplets contain some of the ablated material and ultimately produce ions in an ESI process.

(33) Shia, J. T.; Wang, C. H. *J. Mass Spectrom.* **1997**, *32*, 247–250.

ablation from the target (in the absence of a matrix) with minimal surface damage.[8,24] It is also noted that in ELDI, a relatively close proximity of the sample to the spray plume (3 mm) is required for sufficient ionization. Mid-IR laser ablation of water-rich targets (e.g., in LAESI) is fundamentally different from the UV ablation of organic solids (e.g., nonresonant in ELDI and resonant in MALDI). With the use of linear absorption coefficients, in UV-MALDI the penetration depth of the laser light was estimated at ~300 nm, whereas in mid-IR laser ablation it was ~5 μm. Because of the nonlinear absorption properties of water however, deeper light penetration was demonstrated.[34] Furthermore, enhanced material removal was observed due to the phase explosion induced by Q-switched mid-IR (~3 μm) lasers above ~0.1 J/cm^2.[12] The combined effect of nonlinear absorption and phase explosion results in a two-stage mid-IR ablation process characteristic for water-rich targets.[17,35] Analysis of ELDI and LAESI samples for the degree of laser damage after ablation could further clarify this distinction. Additional differences stem from the operation of the ESI source. In ELDI, there is no control over the spraying regime, whereas in LAESI the spray is operated in the cone−jet mode that produces smaller droplets and higher ionization efficiency.

DISCUSSION

Mid-infrared LAESI is a novel ambient mass spectrometric ion source for biological and medical samples and organisms with sufficient water content. Beyond the benefits demonstrated in the Results section, it offers further, yet untested, possibilities. Unlike imaging with UV-MALDI,[36] it does not require the introduction of an external matrix; thus, the intricacies associated with the application of the matrix coating are avoided and no matrix effects are expected. With an increase in the pulse energy of the ablating laser, it can be used to remove surface material and perform analysis at larger depths. Alternating between material removal and analysis can yield depth profile information. With improved focusing of the laser beam or ultimately with near-field optics, these manipulations can be made more precise and result in better spatial resolution. Reducing the size of the interrogated spot can open new possibilities with the eventual goal of subcellular analysis. These efforts have to be balanced by the sacrifices made in sensitivity due to the smaller amount of material available for analysis. Because of the efficiency of postionization in LAESI, however, the attainable minimum spot size is expected to be smaller than in, for example, AP IR-MALDI.

An inherent limitation of LAESI is its dependence on the water content of the sample. Thus, tissues with lower mid-IR absorbances (e.g., dry skin, bone, nail, and tooth) require significantly higher laser fluences to ablate. This effect is exaggerated by the higher tensile strength of these tissues that suppresses the recoil induced particle ejection. Furthermore, variations of water content and/or tensile strength in a sample can also lead to changes in LAESI ion yield and influence imaging results.

On the basis of our understanding of the LAESI mechanism, additional improvements in ion yield can be expected from enhancing the interaction between the laser ablation and the electrospray plumes. For example, tubular confinement of the ablation plume can make it more directed and increase its overlap with the electrospray. Adjusting the laser wavelength to other (CH or NH) absorption bands can introduce additional channels for laser energy deposition for resonant ablation, thereby enabling the analysis of biological samples with low water content.

Regarding the potential imaging capabilities of LAESI, our experiments suggest that the resolution is determined by the ablation spot size. In imaging LAESI, the laser fluence can be adjusted to completely remove the sample from the interrogated area or the laser irradiation can be turned off while rastering the surface. Thus, spot-to-spot cross contamination can be minimized or eliminated. Depending on surface and analyte properties, these issues are known challenges for DESI imaging.[10]

The current and anticipated unique capabilities of LAESI promise to benefit the life sciences in metabolomics, screening, and imaging applications including the possibility of in vivo studies.

ACKNOWLEDGMENT

This work was supported by the U.S. National Science Foundation under Grant No. 0719232 by the U.S. Department of Energy (DEFG02-01ER15129) and by the W. M. Keck Foundation (041904). Any opinions, findings, and conclusions or recommendations expressed in this material are those of the authors and do not necessarily reflect the views of the supporting organizations.

Received for review June 4, 2007. Accepted August 8, 2007.

AC071181R

(34) Shori, R. K.; Walston, A. A.; Stafsudd, O. M.; Fried, D.; Walsh, J. T. *IEEE J. Sel. Top. Quantum Electron.* **2001**, *7*, 959−970.

(35) Vertes, A. In *Laser Ablation and Its Applications*; Phipps, C. R., Ed.; Springer: New York, 2007; Vol. 129, pp 505−528.

(36) Stoeckli, M.; Chaurand, P.; Hallahan, D. E.; Caprioli, R. M. *Nat. Med.* **2001**, *7*, 493−496.